Design and Analysis of an Outer-rotor Flux-switching DC-field Machine for In-wheel Light Traction

Libing Cao*, K. T. Chau†, Christopher H. T. Lee, and C. C. Chan*****

Abstract – In this paper, an outer-rotor flux-switching DC-field (OR-FSDC) machine for in-wheel light traction is proposed. The machine topology and operation principle are introduced, while the selection principle of stator sections and rotor poles is also investigated. Furthermore, an analytical torque-sizing equation is derived to demonstrate the relationship of key dimensional parameters and machine performances at the preliminary design stage. Consequently, the machine dimensional parameters are optimized to maximize the steady electromagnetic torque and minimize the torque ripple by adopting multi-objective genetic algorithm (MOGA). The machine electromagnetic performances are analyzed based on the time-stepping finite element method (TS-FEM), and hence verifying the validity of design and optimization method.

Keywords: DC-field, Finite element analysis (FEA), Flux-switching, Multi-objective genetic algorithm (MOGA), Outer-rotor.

1. Introduction

With an increasing concern on environmental protection and traffic agility in urban areas, the electric-propelled light traction vehicles without tailpipe emission and bulky size, such as electric motorcycles and bicycles, are greatly in demand in many cities [1]. As the core parts of these electric vehicles (EVs), electric machines are expected to operate with high efficiency, high power density, high torque density, wide-speed range and free maintenance [2-4]. The permanent-magnet (PM) machines, which achieve most of the requirements, have been widely investigated by researchers. Based on the location of PM materials, the PM machines can be classified as three major types, namely the rotor-PM machine, stator-PM machine, dual-PM machine [5-7]. Compared with other two types, stator-PM machines have robust rotor structure and favorable heat dissipation condition [8], [9], and hence received more and more attention, including topology design [10], [11], analysis methods [12], [13], harmonics current injection operation [14-16], control strategies [17], [18]. As one kind of stator-PM machines, the flux-switching permanent magnet (FSPM) machine has been regarded as the most promising candidate for EVs [19-21].

In addition, with adoption of outer-rotor structure, the FSPM machine is desirable for the in-wheel low-speed light traction [22-24]. However, FSPM generally suffers from low cost-effectiveness with usage of rare-earth PM, ineffective flux-controllability and potential PM irreversible demagnetization [25-27]. To improve these problems, the independent DC excitation concept is implemented into the FSPM machine [28-32].

In this paper, by replacing the DC-field windings with PMs in the outer-rotor FSPM machine, and hence the outer-rotor flux-switching DC-field (OR-FSDC) machine is proposed for in-wheel light traction application. The design criteria, parameters optimization and machine performances will be discussed and analyzed in the following sections.

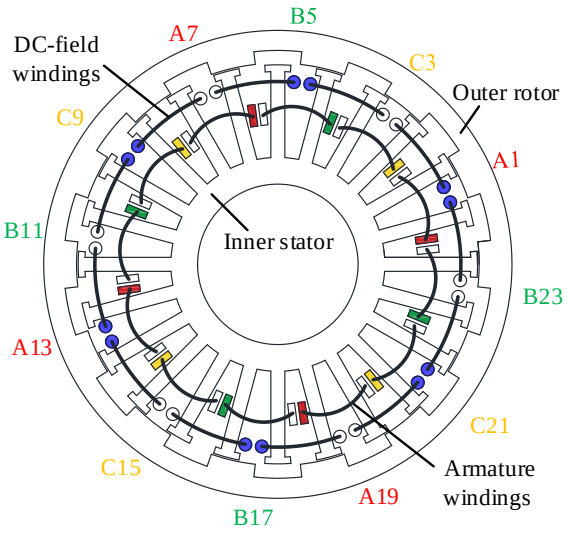

Fig. 1. Cross section of the proposed three-phase wound-field 12s/14r OR-FSDC machine.

2. Machine Topology

Fig. 1 shows the cross section of proposed three-phase wound-field 12-stator-section/14-rotor-pole (12s/14r) OR-

† Corresponding Author: Dept. of Electrical and Electronic Engineering, The University of Hong Kong, Hong Kong (ktchau@eee.hku.hk)

* Dept. of Electrical and Electronic Engineering, The University of Hong Kong, Hong Kong (lbcao@eee.hku.hk)

** Research Laboratory of Electronics, Massachusetts Institute of Technology, Cambridge, USA (chtlee@mit.edu)

***Dept. of Electrical and Electronic Engineering, The University of Hong Kong, Hong Kong (ccchan@eee.hku.hk)

FSDC machine, which comprises an inner stator and an outer rotor. Instead of the toroidal-field topology, wound-field configuration is adopted here. This is because the DC-field close to stator outer surface will not goes through the rotor but outside of the stator in the toroidal-field counterpart, i.e., the proposed wound-field FSDC machine has smaller flux leakage effect [33]. As shown in the cross-section view, the inner stator consists of 24 teeth, on which both DC-field and armature winding are wound in every other stator slot while the rotor is simply iron core with salient poles. It should be noted that two adjacent tooth and their corresponding armature windings form a stator section, which means there are 12 stator sections in the proposed machine.

3. Operating Principle

Fig. 2 shows the operation principle of the proposed 12s/14r OR-FSDC machine under electric degree θ_e. The relationship between θ_e and the mechanical degree θ_m is governed by

$$\theta_e = N_r \theta_m \tag{1}$$

where N_r is the number of rotor iron poles.

In Fig. 2(a), the flux linkage of the coil A1 Φ_{A1} in the inner stator is positive maximum at θ_e =0°. When θ_e = 90°, as shown in Fig. 2(b), Φ_{A1} is 0 since the excitation flux bypasses the coil A1. In Fig. 2(c), Φ_{A1} reaches negative maximum as rotor rotates to θ_e =180°. Again, Φ_{A1} becomes 0 when θ_e =270°, as shown in Fig. 2(d). Therefore, the proposed OR-FSDC machine exhibits bipolar flux linkage.

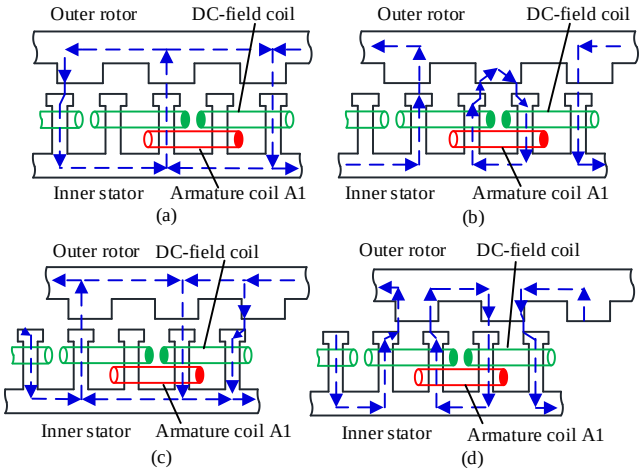

Fig. 2. Operating principles of the proposed OR-FSDC machine. (a) θ_e =0°. (b) θ_e =90°. (c) θ_e =180°. (d) θ_e =270°.

4. Selection of Stator Sections and Rotor Poles Numbers

Similar to the conventional FSPM machines, the stator sections number N_s should be an even and multiple of phase number m. In addition, the rotor poles number N_r should be closer to the stator sections number to obtain larger fundamental pitch factor, whilst larger torque can be achieved by selecting relative higher rotor poles number [34]. Furthermore, the rotor poles number is preferable to an even one since the machine with odd rotor poles exhibits unbalanced magnetic pull. Thus, 14 rotor poles are chosen for the three-phase 12-stator-section OR-FSDC machine, which is denoted as 12s/14r OR-FSDC machine.

In order to have further understanding of the operation principle and calculate the winding factor, the back-EMF phasors for the proposed 12s/14r OR-FSDC machine is shown in Fig. 3.

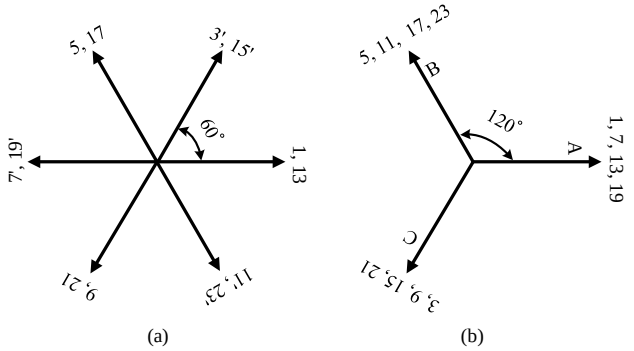

Fig. 3. Back-EMF phasors of the proposed machine. (a) Slot EMF vectors (elec. deg.). (b) Phase coils connection

Based on the phase coils connection, the fundamental distribution factor k_d =1 while the pitch factor v th harmonic is

$$k_{pv} = \left| \sin \frac{2\pi \frac{N_r}{N_s} v + \pi}{2} \right| \tag{2}$$

where 180° electric degree (π rad) is caused by the reversed polarities of adjacent DC-field generated by the field windings and is denoted by n' in Fig. 3(a). Hence, the winding factor k_w can be given by

$$k_w = k_d k_{pv} \tag{3}$$

For the proposed 12s/14r machine, the fundamental winding factor $k_w = \left| \sin \frac{2\pi \frac{14}{12} + \pi}{2} \right| = 0.866$, which is acceptable. Moreover, from the slot EMF vectors in Fig. 3 (a), it can be deduced that all the even harmonics in the coil flux linkages and back-EMF can be cancelled such as coil A1 and coil A7 since there is 180° electric degree displacement between them. Consequently, the phase winding flux linkage and back-EMF exhibit inherently symmetric sinusoidal waveforms. Thus, the proposed OR-

FSDC machine prefers to operate in brushless AC (BLAC) mode. The waveforms and further analyses of flux linkages and back-EMF of proposed machine will be given in Section 7.

5. Torque-Sizing Equations

Similar as other types of machines in the primary design stage, the torque-sizing equations are of great importance since they can offer reference for choosing appropriate machine design parameters at preliminary design stage, which will also be further optimized in Section 6.

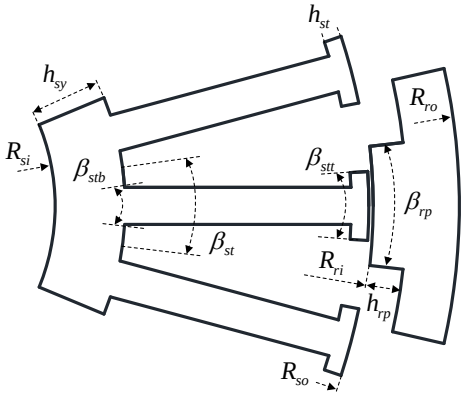

Fig. 4. Design dimensional parameters of the proposed OR-FSDC machine.

Fig. 4 shows the key design dimensional parameters of the proposed machine. The stator tooth bottom arc β_{stb}, stator tooth tip arc β_{stb} and stator tooth arc β_{st} are initially set as

$$\beta_{stb} = \beta_{stt} = \frac{\beta_{st}}{2} = \frac{1}{2}\frac{2\pi}{N_{st}} \tag{4}$$

where N_{st} is the stator teeth number. In addition, the stator inner radius R_{si} and stator outer radius R_{so} are initially set as $R_{si} = 0.4R_{so}$ in order to provide sufficient space for the DC-field and armature windings. Furthermore, to achieve the distribution balance of magnetic flux density between the stator teeth and yoke, stator yoke thickness is set as

$$h_{sy} = R_{sy} - R_{si} = 2\beta_{stb}R_{sy} \tag{5}$$

where R_{sy} is the radius of stator yoke. Then, the stator tooth thickness h_{st} is initially set as $\frac{1}{4}\beta_{stt}R_{so}$ to avoid over-saturation in the stator tooth. Based on the above dimensions, the slot area for windings S_w can be deduced by

$$S_w = \frac{1}{2}\beta_{st}(R_{so} - h_{st})^2 - \frac{1}{2}\beta_{st}R_{sy}{}^2 - \beta_{stb}R_{sy}(R_{so} - h_{st} - R_{sy})^2 \tag{6}$$

In terms of the rotor, the rotor pole arc β_{rp} is initially set by $\beta_{rp} = \frac{1}{2}\frac{2\pi}{N_r}$, denoting that the rotor pole arc and slot arc are equal. Besides, the rotor pole height h_{rp} is set as $2h_{st}$ to achieve sufficient rotor saliency whilst the rotor yoke thickness h_{ry} is initially set as $\frac{3}{2}h_{rp}$ to obtain enough mechanical strength and distribution balance of magnetic flux density between the rotor poles and yoke. Hence, the rotor outer radius R_{ro} can be determined by

$$R_{ro} = h_{ry} + h_{rt} + R_{so} + g = (\frac{5}{4}\beta_{stt} + 1)R_{so} + g \tag{7}$$

Due to the essentially sinusoidal phase back-EMF waveform, as stated in Section 4, the coil back-EMF can be expressed as [22]

$$e_{coil} = N_{ac}\omega N_r k_{sat} k_l \Phi_m \sin(N_r\theta_r) \tag{8}$$

where N_{ac} is the armature coil turns number, ω is the mechanical rotational speed, Φ_m is the maximum armature coil DC-field flux at open-circuit condition, k_{sat} and k_l are the saturation and leakage factors. It should be noted that k_{sat} and k_l are considered to be 1 in the ideal situation and become smaller with the increase of saturation and flux leakage. Meanwhile, Φ_m can be obtained by

$$\Phi_m = 2B_{ma}l\frac{2\pi R_{so}}{N_{st}} \tag{9}$$

where B_{ma} is the average open-circuit air-gap flux density at d-axis as shown in Fig. 2 (a).

Hence, the maximum value of coil back-EMF E_{coil} can be deduced

$$E_{coil} = \frac{4\pi R_{so}}{N_{st}} N_{ac}\omega N_r k_{sat} k_l B_{ma} l \tag{10}$$

The maximum value of phase back-EMF

$$E_{phase} = \frac{N_{st}}{2m}E_{coil} \tag{11}$$

Besides, the maximum phase current I_{phase} is

$$I_{phase} = \frac{J_p k_f S_w}{2N_{ac}} \tag{12}$$

where J_p is the rated current density and k_f is the stator slot filling factor.

Therefore, the electromagnetic power P_e is deduced by

$$P_e = \frac{m}{2}E_{phase}I_{phase} = \frac{\pi R_{so}}{2}\omega N_r k_{sat} k_l B_{ma} l J_p k_f S_w \tag{13}$$

Then, the electromagnetic torque T_e is obtained by

$$T_e = \frac{P_e}{\omega} = \frac{\pi R_{so}}{2}N_r k_{sat} k_l B_{ma} l J_p k_f S_w \tag{14}$$

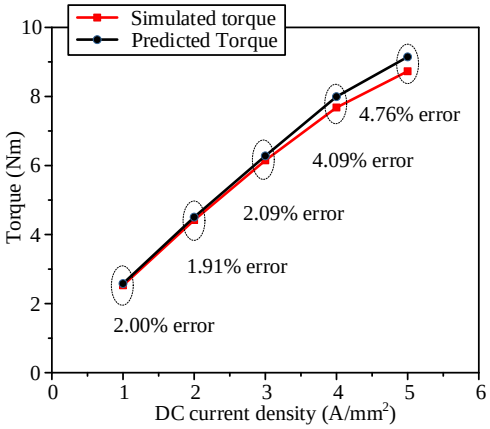

Fig. 5. Steady torque under different DC winding current densities.

Table 1. Preliminary Design Parameters of the Proposed Machine

Parameter	Unit	value
Rotor outer radius R_{ro}	mm	70
Rotor inner radius R_{ri}	mm	60.2
Stator outer radius R_{so}	mm	59.7
Stator inner radius R_{si}	mm	24
Air-gap length g	mm	0.5
Active stack length l	mm	100
Rotor pole height h_{rp}	mm	3.9
Rotor pole arc β_{rp}	°	12.86
Stator teeth thickness h_{st}	mm	1.95
Stator teeth tip arc β_{stt}	°	7.5
Stator teeth bottom arc β_{stb}	°	7.5
Stator yoke thickness h_{sy}	mm	8.5
Stator slot filling factor k_f	-	0.6
DC-field winding turns N_{dc}	-	60
Turns number per coil in series N_{ac}	-	12
Turns number per coil in parallel N_{acp}	-	5
Rated current density J_p	A/mm^2	5
Rated speed	rpm	150
Stator sections number	-	12
Rotor poles number	-	14

Based on the above electromagnetic torque equation and FEM analysis, the steady predicted and simulated torque are achieved under armature rated current density 5 A/mm^2, respectively, which are shown in Fig. 5. One can see that the predicted torque is slightly larger than the simulated torque whilst their discrepancies increase with larger injected DC current density. This is mainly due to the saturation and flux leakage effect. However, the errors are acceptable. Thus, the derived torque-sizing equation shows satisfactory accuracy and can offer a proper reference at the preliminary design stage.

Then, according to the required electromagnetic torque and other constraints, the key design dimensions of proposed OR-FSDC machine can be predetermined based on (7) and (14). For the proposed OR-FSDC machine, Table I lists the preliminary design parameters of proposed machine, which are be further optimized in the following section.

6. Design Optimization

In this section, the machine design parameters are optimized in order to obtain larger electromagnetic torque and smaller peak-to-peak torque ripple under the same copper loss. Since the stator teeth thickness h_{st}, stator teeth tip arc β_{stt}, rotor pole height h_{rp} and rotor pole arc β_{rp} significantly influence average torque and torque ripple, all these parameters will be taken into consideration. In addition, due to the relative larger numbers of these parameters and their coupled influence on the optimization objectives, the multiple-objective genetic algorithm (MOGA) coupled with finite element analysis (FEA) is adopted to optimize these parameters in the commercial FEM-based software - JMAG designer.

Table 2. Optimization Parameters of the Proposed Machine

Parameter	Lower limit	Upper limit	Optimized
β_{rp}	10.28°	15.43°	10.94°
h_{rp}	3.12mm	4.68mm	4.67mm
β_{stt}	6°	9°	8.44°
h_{st}	1.56mm	2.34mm	1.57mm

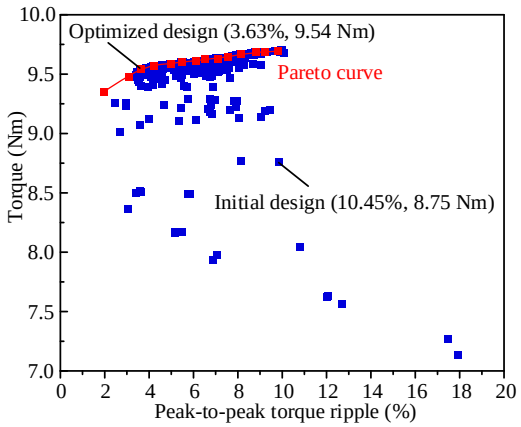

Fig. 6. Optimization between steady torque and torque ripple based on MOGA.

Table 2 shows the optimization parameters and their optimization values. It should be noted that the variation range of all these parameters are set as 0.8~1.2 times of parameters initial values. Meanwhile, Fig. 6 shows the optimization pareto curve to maximize the steady torque and minimize the torque ripple under rated current density 5 A/mm^2. With the coupled FEA and MOGA optimization, the average torque is enhanced by 9.03% whilst the peak-to-peak torque ripple is significantly decreased by 65.26%,

7. Electromagnetic Performance Analysis

Based on the optimization results, the electromagnetic performances are analyzed and compared with those in the initial design including cogging torque, steady torque, coil flux linkage and coil back-EMF.

Firstly, Fig. 7 (a) and Fig. 7 (b) show the cogging torque and steady torque waveforms of initial and optimized design, respectively. One can find that the peak value of cogging torque is also significantly decreased by 89.47% after optimization from 0.19 Nm to 0.02 Nm. In addition, the number of the cogging torque cycles per electric period n_e can be calculated by

$$n_e = \frac{LCM(N_s, N_r)}{N_r} = 6 \tag{13}$$

where *LCM* denotes the least common multiple number. Hence, the calculated cogging torque cycles per electric period is identical to that of cogging torque waveforms. Furthermore, the steady torque and torque ripple is improved as shown in Fig. 6 and Fig. 7 (b).

Secondly, the coil flux linkages waveforms of initial design and optimized design under rated speed are shown in Fig. 8 (a) and Fig. 8 (b), respectively. Since the coils of phase A, namely, A13 and A1, A7 and A19 are periodically identical, only coil A1 and A7 are analyzed. It can be seen that the flux linkages of coil A1 and coil A7 are slightly asymmetric. However, the consequent coil A1+A7 exhibit symmetric sinusoidal waveforms as the even harmonics are cancelled as stated in Section 4.

Finally, the coil back-EMF waveforms of initial design and optimized design under rated speed are analyzed, as depicted in Fig. 9 (a) and Fig. 9 (b), respectively. It can be seen that similar results can be obtained as the coil flux linkages. Furthermore, the spectra of the coil back-EMF are also analyzed as shown in Fig. 10. One can find that all the even harmonics of coil A1 and coil A7 are cancelled in coil A1+A7. In addition, the 3th harmonic order is zero in coil A1, coil A7 and coil A1+coil A7. This is because the 3th pitching factor k_{p3} is calculated by

$$k_{p3} = \left| \sin \frac{2\pi \frac{14}{12} \times 3 + \pi}{2} \right| = 0 \tag{14}$$

In addition, after optimization, the total harmonic distortion (THD) is decreased from 5.42% to 4.27%.

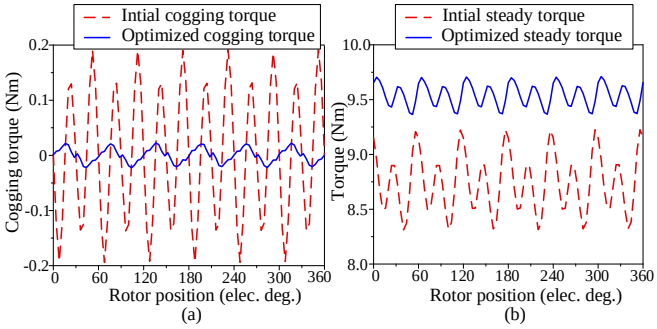

Fig. 7. Torque waveforms of initial and optimized designs. (a) Cogging torque. (b) Steady torque.

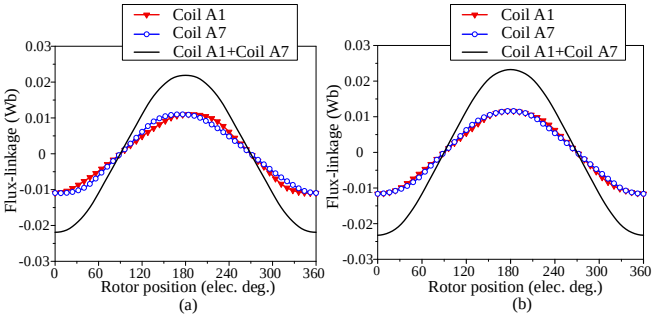

Fig. 8. Flux linkages waveforms of initial and optimized designs. (a) Initial design. (b) Optimized design.

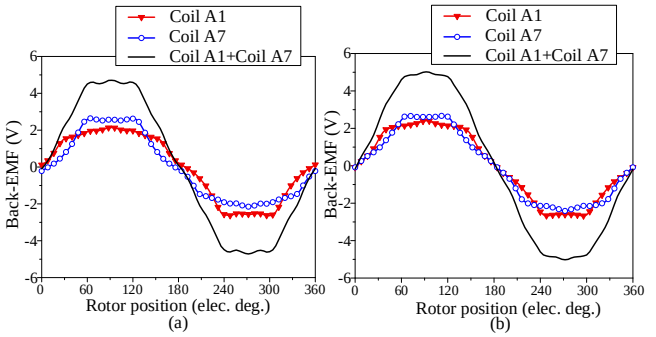

Fig. 9. Back-EMF waveforms of initial and optimized designs. (a) Initial design. (b) Optimized design.

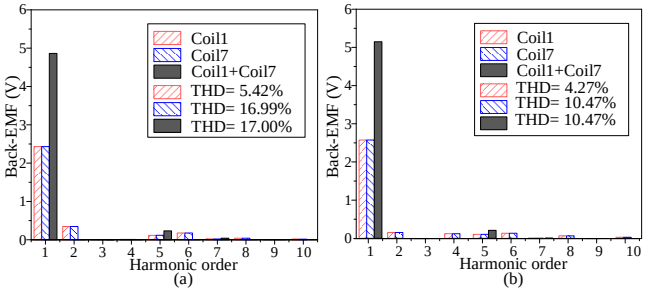

Fig. 10. Spectra of coil back-EMF waveforms of initial and optimized designs. (a) Initial design. (b) Optimized design.

8. Conclusion

This paper proposes an OR-FSDC machine for in-wheel light traction, with emphasis on machine design and analysis. Based on the machine topology and operation principle, the torque-sizing equation is derived for the proposed machine, which shows satisfactory accuracy and offers a proper reference at the preliminary design stage. Then, the machine parameters are optimized to achieve maximum average torque and minimum torque ripple by adopting MOGA instead of traditional optimization method. Finally, the torque-sizing equation and MOGA optimization method are verified by using TS-FEM.

Acknowledgements

This work was supported by the Hong Kong Research Grants Council, Hong Kong Special Administrative Region, China [Project number 17200614].

References

[1] P. Mulhall, S. M. Lukic, S. G. Wirasingha, Y. J. Lee, and A. Emadi, "Solar-assisted electric auto rickshaw three-wheeler," *IEEE Trans. Veh. Technol.*, vol. 59, pp. 2298-2307, 2010.

[2] K. T. Chau, C. C. Chan, and C. Liu, "Overview of permanent-magnet brushless drives for electric and hybrid electric vehicles," *IEEE Trans. Ind. Electron.*, vol. 55, pp. 2246-2257, 2008.

[3] Z. Q. Zhu and D. Howe, "Electrical machines and drives for electric, hybrid, and fuel cell vehicles," *Proc. IEEE*, vol. 95, pp. 746-765, 2007.

[4] K.T. Chau and W. Li, "Overview of electric machines for electric and hybrid vehicles," *International Journal of Vehicle Design*, vol. 64, no. 1, pp. 46-71, 2014.

[5] K. T. Chau, Electric Vehicle Machines and Drives: Design, Analysis and Application, *Wiley-IEEE Press*, 2016.

[6] M. Cheng, K. T. Chau, and C.C. Chan, "Design and analysis of a new doubly salient permanent magnet motor," *IEEE Trans. Magn*., vol. 37, pp. 3012-3020, 2001.

[7] Q. Wang, S. Niu, and L. Yang, "Design Optimization and Comparative Study of Novel Dual-PM Excited Machines," *IEEE Trans. Ind. Electron.*, vol. 64, pp. 9924-9933, 2017.

[8] C. Liu, K.T. Chau, J.Z. Jiang and S. Niu, "Comparison of stator-permanent-magnet brushless machines," *IEEE Trans. Magn*., vol. 44, no. 11, pp. 4405-4408, Nov. 2008,

[9] M. Cheng, W. Hua, J. Zhang, and W. Zhao, "Overview of stator-permanent magnet brushless machines," *IEEE Trans. Ind. Electron.*, vol. 58, pp. 5087-5101, 2011.

[10] X. Zhu, K.T. Chau, M. Cheng and C. Yu, "Design and control of a flux-controllable stator-permanent magnet brushless motor drive," *AIP Journal of Applied Physics*, vol. 103, no. 7, paper no. 7F134, pp. 1-3, Apr. 2008.

[11] K.T. Chau, D. Zhang, J.Z. Jiang, C. Liu and Y.J. Zhang, "Design of a magnetic-geared outer-rotor permanent-magnet brushless motor for electric vehicles," *IEEE Trans. Magn*. vol. 43, no. 6, pp. 2504-2506, Jun. 2007,

[12] Y. Du, F. Xiao, W. Hua, X. Zhu, M. Cheng, L. Quan, K.T. Chau, "Comparison of flux-switching PM motors with different winding configurations using magnetic gearing principle," *IEEE Trans. Magn*., vol. 52, no. 5, paper no. 8201908, pp. 1-8, May 2016.

[13] L. Mo, L. Quan, X. Zhu, Y. Chen, H. Qiu and K.T. Chau, "Comparison and analysis of flux-switching permanent-magnet double-rotor machine with 4QT used for HEV," *IEEE Trans. Magn*., vol. 50, no. 11, paper no. 8205804, pp. 1-4, November 2014.

[14] W. Zhao, M. Cheng, K.T. Chau, R. Cao and J. Ji, "Remedial injected harmonic current operation of redundant flux-switching permanent magnet motor drives," *IEEE Trans. Ind. Electron.*, vol. 60, no. 1, pp. 151-159, Jan. 2013,

[15] X. Zhu, M. Cheng, K.T. Chau and C. Yu, "Torque ripple minimization of flux-controllable stator-permanent-magnet brushless motors using harmonic current injection," *J. Appl. Phys.*, vol. 105, no. 7, paper no. 07F102, pp. 1-3, Apr. 2009,

[16] W. Zhao, M. Cheng, K.T. Chau and C.C. Chan, "Control and operation of fault-tolerant flux-switching permanent-magnet motor drive with second harmonic current injection," *IET Electric Power Appl.*, vol. 6, no. 9, pp.707-715, Nov. 2012,

[17] W. Zhao, M. Cheng, K.T. Chau, W. Hua, H. Jia, J. Ji and W. Li, "Stator-flux-oriented fault-tolerant control of flux-switching permanent-magnet motors," *IEEE Trans. Magn*., vol. 47, no. 10, pp. 4191-4194, Oct. 2011.

[18] M. Cheng, F. Yu, K.T. Chau, and W. Hua, "Dynamic performance evaluation of a nine-phase flux-switching permanent magnet motor drive with model predictive control," *IEEE Trans. Ind. Electron.*, vol. 63, no. 7, pp. 4539-4549, Jul. 2016.

[19] C.H.T. Lee, W.K. Lee, and K.T. Chau, "Development of partitioned stator flux-switching machines for electric vehicles," *Journal of International Council on Electrical Engineering*, vol. 7, no. 1, pp. 276-281, 2017.

[20] W. Hua, G. Zhang, and M. Cheng, "Analysis of two novel five-phase hybrid-excitation flux-switching machines for electric vehicles," *IEEE Trans. Magn*, vol. 50, pp. 1-5, 2014.

[21] C. H. T. Lee, J. L. Kirtley, and M. Angle, "A partitioned-stator flux-switching permanent-magnet machine with mechanical flux adjusters for hybrid electric vehicles," *IEEE Trans. Magn.*, vol. 53, pp. 3000807, 2017.

[22] W. Hua, H. Zhang, M. Cheng, J. Meng, and C. Hou, "An outer-rotor flux-switching permanent-magnet-machine with wedge-shaped magnets for in-wheel light traction," *IEEE Trans. Ind. Electron.*, vol. 64, pp. 69-80, 2017.
[23] Y. Wang, K.T. Chau, C.C. Chan, and J.Z. Jiang, "Transient analysis of a new outer-rotor permanent-magnet brushless dc drive using circuit-field-torque time-stepping finite element method," *IEEE Trans. Magn.*, vol. 38, no. 2, pp. 1297-1300, Mar. 2002.
[24] W. Fei, P. C. K. Luk, J. X. Shen, Y. Wang, and M. Jin, "A novel permanent-magnet flux switching machine with an outer-rotor configuration for in-wheel light traction applications," *IEEE Trans. Ind. Appl.*, vol. 48, pp. 1496-1506, 2012.
[25] I. Boldea, L. N. Tutelea, L. Parsa, and D. Dorrell, "Automotive electric propulsion systems with reduced or no permanent magnets: An overview," *IEEE Trans. Ind. Electron.*, vol. 61, pp. 5696-5711, 2014.
[26] C. H. T. Lee, K. T. Chau, C. Liu, and C. C. Chan, "Overview of magnetless brushless machines," *IET Electric Power Appl.*, DOI: 10.1049/iet-epa.2017.0284.
[27] Q. Wang and S. Niu, "Overview of flux-controllable machines: Electrically excited machines, hybrid excited machines and memory machines," *Renewable & Sustainable Energy Reviews*, vol. 68, pp. 475-491, Feb. 2017.
[28] C.H.T. Lee, K.T. Chau, and C. Liu, "Design and analysis of a dual-mode flux-switching doubly salient DC-field magnetless machine for wind power harvesting," *IET Renewable Power Generation*, vol. 9, no. 8, pp. 908-915, Nov. 2015.
[29] F. Lin, K.T. Chau, C.H.T. Lee, and C. Liu, "Fault signature of a flux-switching DC-field generator," *IEEE Trans. Magn.*, vol. 51, no. 11, paper no. 8206304, pp. 1-4, Nov. 2015.
[30] C. H. T. Lee, K. T. Chau, and C. Liu, "Design and analysis of an electronic-geared magnetless machine for electric vehicles," *IEEE Trans. Ind. Electron.*, vol. 63, pp. 6705-6714, 2016.
[31] Z. Q. Zhu, Z. Z. Wu, D. J. Evans, and W. Q. Chu, "A wound field switched flux machine with field and armature windings separately wound in double stators," *IEEE Trans. Energy. Convers.*, vol. 30, pp. 772-783, 2015.
[32] C.H.T. Lee, K. T. Chau, C. Liu, and F. Lin, "Design and analysis of a magnetless flux-switching DC-excited machine for wind power generation," *Journal of International Council on Electrical Engineering*, vol. 4, no. 1, pp. 80-87, Jan. 2014,
[33] Y. Tang, J. Paulides, T. Motoasca, and E. Lomonova, "Flux-switching machine with DC excitation," *IEEE Trans. Magn.*, vol. 48, pp. 3583-3586, 2012.
[34] J. Chen and Z. Zhu, "Winding configurations and optimal stator and rotor pole combination of flux-switching PM brushless AC machines," *IEEE Trans. Energy. Convers.*, vol. 25, pp. 293-302, 2010.

Libing Cao received the B.Eng. degree in Electrical and electronic engineering from Zhejiang University, Hangzhou, China, in 2016. He is currently working toward the Ph.D. degree in electrical and electronic engineering in The University of Hong Kong, Hong Kong. His research interests include electric machines and drives, magnetic gears, electric vehicle technologies. Mr. Cao received the Hong Kong PhD Fellowship in 2016 to support his PhD study.

K. T. Chau received his BSc (Eng.) degree with first class honors, MPhil degree, and PhD degree from The University of Hong Kong, Hong Kong, all in electrical and electronic engineering. He joined the alma mater in 1995, and currently serves as a Professor in the Department of Electrical and Electronic Engineering. His main research interests include electric vehicle technologies, renewable energy systems, and machines and drives. In these areas, he has published 7 books, 9 book chapters, and more than 250 refereed journal papers. Prof. Chau is a Fellow of the IEEE, the IET, and the HKIE. He has served as Chairs and Organizing Committee Member for many international conferences. He has received many awards, including the Chang Jiang Chair Professorship, the Environmental Excellence in Transportation Award for Education, Training and Public Awareness, and the Award for Innovative Excellence in Teaching, Learning and Technology.

Christopher H. T. Lee received his B.Eng. degree with first class honors, and Ph.D. degree both in electrical engineering from Department of Electrical and Electronic Engineering, The University of Hong Kong, Hong Kong. He currently serves as the Postdoctoral Fellow in Research Laboratory of Electronics, Massachusetts Institute of Technology, and also the Honorary Assistant Professor in his alma mater. His research interests are Electric Machines and Drives, Renewable Energies, and Electric Vehicle Technologies. In these areas, he has published 1 book, 3 books chapters, and about 60 referred papers. Dr. Lee has received many awards, including the Li Ka Shing Prize (the best Ph.D. thesis award) and the Croucher Foundation Fellowship to support his postdoctoral research.

C. C. Chan received his B.Sc., M.Sc., and Ph.D. degrees in Electrical Engineering from China University of Mining & Technology, Tsinghua University and The University of Hong Kong, in 1957, 1959 and 1982, respectively. He is currently the Honorary Professor and the former Head of the Department of Electrical and Electronic Engineering, The University of Hong Kong. He has more than 10 years industrial experience and more than 35 years academic experience. He is the President of the HKIE in Session 1999/2000, the Founding President of the International Academy for Advanced Study, China, the Cofounder and Rotating President of the World Electric Vehicle Association, and the President of the Electric Vehicles Association of Asia Pacific. He is the Honorary Fellow of the HKIE, Fellow of the IEEE, the IET, the Royal Academy of Engineering at the UK, the Chinese Academy of Engineering, and The Ukraine Academy of Engineering Sciences. His major honors include the awards of the HKIE Gold Medal in 2010, World Federation of Engineering Organizations (WFEO) Medal of Engineering Excellence in 2013, the Royal Academy of Engineering Prince Phillip Medal in 2014, and the Guanghua Engineering Science and Technology Award in 2016.